Morphology of polyacetylene and doped polyacetylene

A. J. Epstein, H. Rommelmann. R. Fernquist and H. W. Gibson
Xerox Corporation, Joseph C. Wilson Center for Technology, 800 Phillips Road — W114, Webster, New York 14580, USA

M. A. Druy* and T. Woerner
Department of Chemistry, University of Pennsylvania, Philadelphia, Pennsylvania 19104, USA
(*Received* 18 *June* 1981; *revised* 1 *October* 1981)

A detailed study of the morphology of polyacetylene and iodine and arsenic pentafluoride doped polyacetylene has been carried out using scanning electron microscopy and transmission electron microscopy techniques. The results reveal a variety of fibrillar and rod-like morphologies for *trans*-polyacetylene. The samples retain this morphology upon doping, with, in many cases, a significant increase in the diameter of these structures. Larger increases in diameter were observed for the AsF_5 doped samples than in iodine doped samples. Energy dispersive X-ray analysis and back-scattered electron imaging were used to determine dopant distribution. Both iodine and arsenic distributions were uniform across the film surfaces to a resolution of 5000 Å. In addition, both dull and shiny sides of the films are shown to have approximately the same dopant concentration. This demonstrates that nonuniformity of the doping occurs, if at all, at a much finer scale. Finally, we have determined that small crystals, presumably arsenic trioxide, form on the surface of AsF_5 doped polyacetylene upon even moderate exposure to air.

Keywords Polyacetylene; doped polyacetylene; conducting polymers; morphology; dopent homogeniety; scanning electron microscopy

INTRODUCTION

There is extensive current interest in polyacetylene, $(CH)_x$, and the effects of doping it with donors and acceptors. This interest was stimulated by the discovery[1] that doping with donors and acceptors results in more than twelve orders of magnitude increase in the conductivity, σ, and the formation of the metallic state[2].

Acetylene was first polymerized[3] in 1958, in the form of a grey powdery material. The preparation of polyacetylene films[4] in the presence of a Ziegler catalyst (Shirakawa technique) enabled detailed physical studies to be carried out. Both *cis*, and the thermodynamically more stable *trans* isomers, *Figure 1*, can be obtained by this technique. Early transmission electron micrographs (*TEM*) and scanning electron micrographs (*SEM*) established[4] that these polymers had a fibrillar morphology, with fibrils generally having diameters of 200–300 Å. Subsequent study of acetylene polymerized directly onto electron microscope gold grids, confirmed that the nascent morphology of polyacetylene is fibrillar[5]. This fibrillar morphology and the $(CH)_x$ crystallinity were found to vary with preparation technique[6]. The conductivity of the doped samples was also preparation dependent[6].

Recently it has been reported[7] that *cis*-polyacetylene prepared using a dilute Shirakawa catalyst and prepared with Luttinger's[8] catalyst 'consist of irregularly shaped lamellar-like particles of typically a few hundred Å diameter and a thickness of 50–100 Å as the smallest discernible morphological subunit. These subunits are aggregated to a loose network or sponge in a pseudofibrillar arrangement'. *Trans*-polyacetylene has also been obtained by polymerization under shear flow in a Couette-type apparatus[9] (Meyer's method). It is reported[10] to be single-crystal like in character, embedded

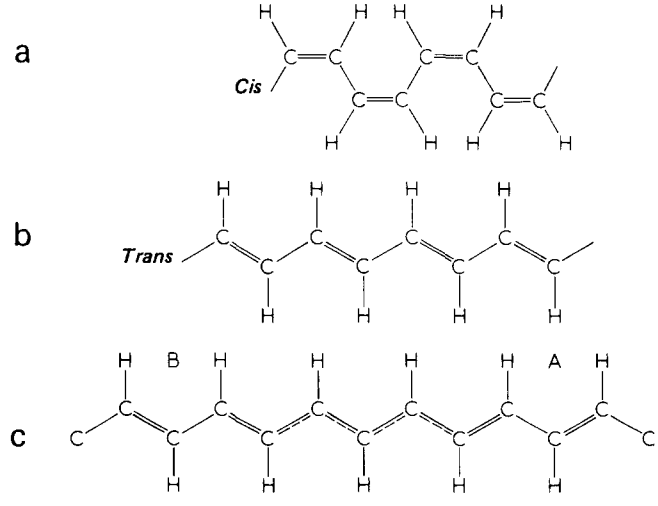

Figure 1 Idealized polyacetylene structures: (a) *cis*-$(CH)_x$; (b) *trans*-$(CH)_x$; (c) a soliton separates two regions (A and B) of bond alternation with opposite phase (schematic)

* Present address: Advanced Technology Laboratory, GTE Laboratories Inc., 40 Sylvan Road, Waltham, MA 02254, USA

0032-3861/82/081211-11$03.00

in material having the usual character of Shirakawa and Luttinger type.

The fibrillar morphology may play an important role in the doping mechanism, the insulator-metal transition and the temperature dependent conductivity in the metallic state. The presence of these fibrils is important for rapid electrochemical doping and the fabrication of lightweight rechargeable storage batteries[11].

Solitons[12,13] or bond alternation defects[14] can occur in *trans*-$(CH)_x$, *Figure 1*. In undoped *trans*-$(CH)_x$ the solution is a domain wall which separates two equivalent structures: one in which the alternating single and double bonds occur in a particular order and a second with the order of the bonds interchanged. This domain wall is electrically neutral and is estimated to be of the order of seven formula units long[13]. The neutral soliton has an energy midway between the filled valence band and empty conduction band, and has a net spin[12-14] associated with it. The spin comes from the unpaired electron in the defect. When the soliton is charged (by adding or removing an electron from the defect), it is spinless. It has been suggested[12,13] that solitons form in *trans*-$(CH)_x$ upon isomerization from *cis*. The soliton levels are the first levels to be oxidized upon doping with acceptors, thereby removing spins. Upon light doping, additional charged solitons are created with a lower cost of energy than creation of holes directly in the valence band[12,13].

Experimental results of magnetic[15,16], infra-red[17], optical[18] and phototransport[19] measurements on AsF_5 doped $(CH)_x$ support the soliton mechanism[12,13] for doping. Alternatively, Tomkiewicz *et al.*[20] argued against soliton formation in $(CH)_x$ on the basis of magnetic susceptibility (χ) measurements of samples doped with AsF_5 to concentration, y, near 1%. On the basis of these measurements, electric field dependent conductivity[21] and *SEM* studies[22], they proposed that the properties of doped $(CH)_x$ are dominated by the formation of metallic islands separated by undoped polymer. The semiconductor–metal transition is then viewed as a percolation of such metallic islands[21,22]. However, on the basis of magnetic[16] and optical[18] measurements on $[CH(AsF_5)_y]_x$ and electric field, frequency and temperature dependent conductivity studies[23,24] and magnetic studies[25,26] of iodine doped $(CH)_x$, it was shown that although the dopant distribution may be nonuniform, it is not segregated into metallic islands. In addition, the temperature and electric field dependence of the conductivity of iodine doped polyacetylene have been interpreted[23,24,27] in terms of the maximum metallic resistance of one- and two-dimensional wires and films with disorder. This model emphasizes the role of the finite cross-section of the polyacetylene fibrils.

It is important to establish the detailed morphology of polyacetylene and the effect of doping on that morphology. It is also important to establish the variation in dopant concentration in these films. An extensive scanning electron microscopic and transmission electron microscopic study has been carried out on polyacetylene and the effects of doping by iodine and AsF_5. Most of the samples studied here were utilized in electric field dependent conductivity experiments[27] and magnetic susceptibility[24] experiments. The results show the presence of the fibrillar morphology in polyacetylene. No significant change of this morphology with doping is observed. A moderate swelling of the fibrils was observed with iodine doping. A much more extensive swelling was observed in the AsF_5 doped system. In addition energy dispersive X-ray analysis (EDXA) demonstrates that there is no significant variation in dopant distribution along the films or between the two sides of the films within the spatial resolution of the EDXA (5000 Å). Back-scattered electron images also revealed no dopant segregation within the resolution of the technique (5000 Å). The *TEM* studies revealed no obvious iodine segregation within the instrumental imaging resolution ($\sim$50 Å).

EXPERIMENTAL

All *SEM* studies were done on a JEOL JXA-35 scanning electron microscope/electron probe X-ray micronalyser except for those reported in *Figures 9b* and *10b* which were carried out on a Philips 501B scanning electron microscope. The former system has a JEOL wavelength dispersive X-ray spectrometer as well as a Kevex 5100 Quantex-ray energy dispersive X-ray analyser for quantitative work (spatial resolution to 5000 Å). The JEOL *SEM* is capable of up to 50 Å image resolution in the secondary electron mode and 1500 Å in the back-scattered mode; the Philips *SEM* is capable of approximately 100 Å image resolution. All samples had thin gold coatings sputtered on prior to viewing. The beam currents were kept sufficiently low to preclude sample damage (less than 1×10^{-10} amps). During the energy dispersive X-ray analysis studies the beam current was 2×10^{-10} amps. With these currents the beam probe diameter at the surface was approximately 200 Å. The maximum temperature increase is estimated to be less than 1 K assuming a stationary beam[28], and a thermal conductivity[29] of 0.5 watt/cm K for polyacetylene. Sample damage was observed for specimen currents of 9×10^{-9} amps. For the *SEM* micrographs shown in the *Figures*, the digits give the conditions at the time of the photograph. The first two digits on the left give the accelerating voltage (in kilovolts). The next three digits give the magnification (e.g., $103 \equiv 10 \times 10^3$). The following four digits are the micrograph number. Finally, the last five digits give the length of the white bar scale in microns.

The *TEM* studies were performed utilizing a Philips EM 301 instrument. Experimental conditions resulted in a resolution of $\sim$40 Å. The samples for *TEM* studies were potted in a Ciba-Geigy 60/20 epoxy resin with Landcast A hardener. After curing, samples were microtomed into approximately 1000–1500 Å thick slices for study.

The samples of polyacetylene film were prepared at Xerox Webster Research Center and at the University of Pennsylvania using the Shirakawa technique[4]. Most of the samples were doped by exposing the $(CH)_x$ to dopant vapour carried by a flow of dry nitrogen gas[12,25]. The heaviest iodine doped sample was achieved by allowing the polyacetylene film to be exposed to excess iodine vapour at room temperature for three days in an argon atmosphere. The samples labelled 'uniformly doped' were prepared by utilizing a slow doping technique developed[16,25] to achieve a homogeneous distribution of dopant ions.

RESULTS AND DISCUSSION

Morphology of trans-$(CH)_x$

Several different preparations of undoped *trans*-

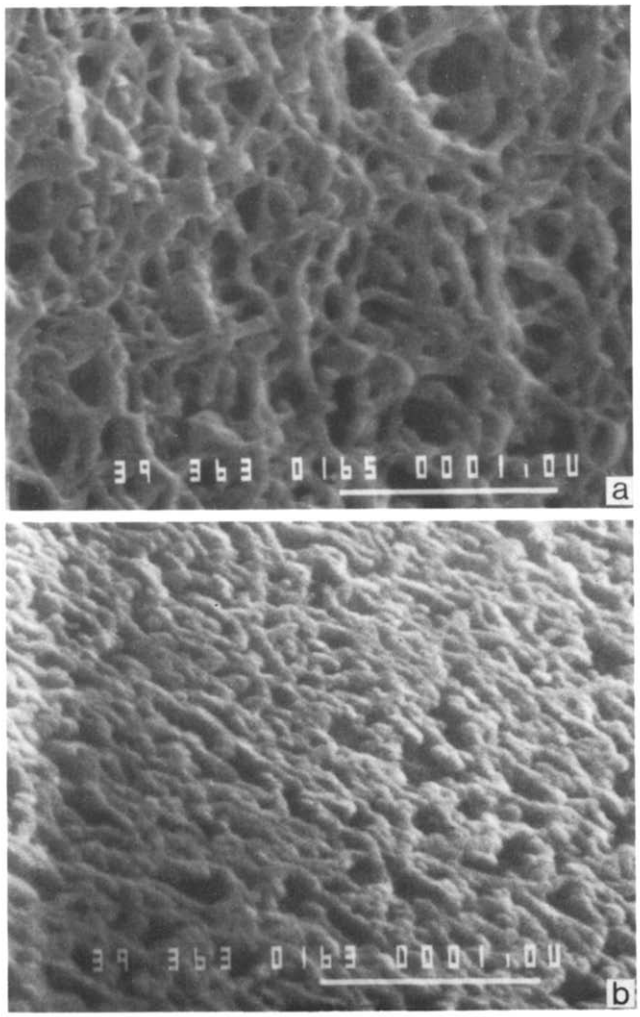

Figure 2 ***SEM*** micrographs of ***trans***-(polyacetylene) prepared at Xerox (a) the dull side; (b) the shiny side. The key to the numbers on these and all subsequent micrographs is the first two digits on the left give the accelerating voltage in kilovolts, the next three digits give the magnification (e.g., 363 ≡ 36 x 10^3), the following four digits are the micrograph number, finally, the last five digits give the length of the white bar scale in microns

polyacetylene were examined in the *SEM* to establish the variation in morphology with preparation. All films studied had a dull side (facing towards the inside of the reactor vessel) and a shiny side (facing the smooth glass wall of the reactor vessel during the polymerization). In general the dull side of the film was very porous, with identifiable fibrils. The shiny side was very smooth with the fibrils matted. In some cases the fibrils were so matted as to make it difficult to distinguish their presence. *Figures 2* through *4* exemplify the variation in morphology observed for the nascent *trans*-polyacetylene.

Figure 2a illustrates the results for the dull side of a sample prepared at the Xerox Webster Research Center. The fibrils are about 500 Å in diameter and extend for several thousands of Angstroms. The shiny side of the same film is seen at the same magnification in *Figure 2b*. Here the fibrils are so crowded that the fibrous nature is nearly masked. Samples from this same film were used to study the effects of extensive iodine doping (*Figure 7*).

A second preparation of *trans*-polyacetylene, prepared at the University of Pennsylvania, is displayed in *Figure 3*. *Figures 3a* and *b* show the dull side under ten thousand and thirty-six thousand magnification. The fibrous network is clearly visible. However, the fibrils in this sample have a diameter of ~200 Å. Occasional pieces of non-fibrous material are observed, as in *Figure 3a*. The shiny side of the same film, depicted in *Figure 3*, reveals a fibrous structure so matted, that it is difficult to identify. Instead it appears to consist of rigid rods. A higher magnification shows the diameter of these 'rods' to be

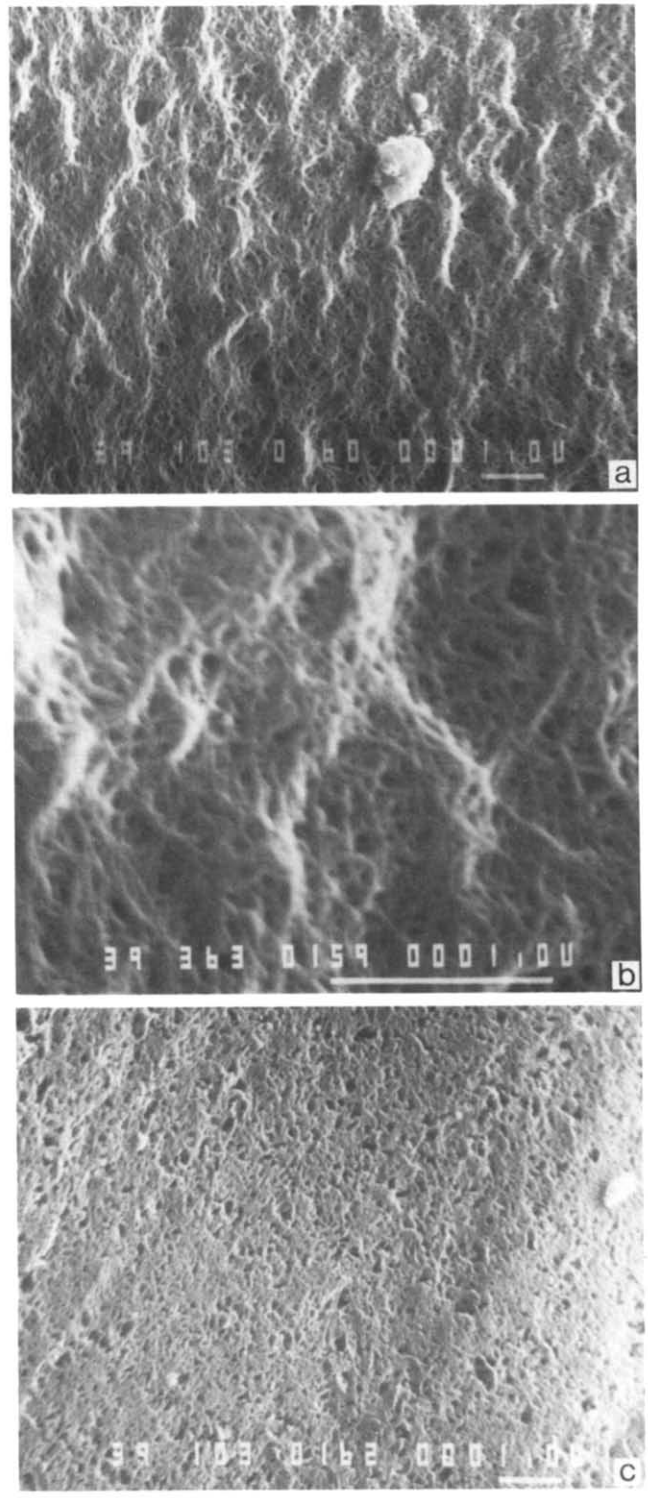

Figure 3 *Trans*-polyacetylene prepared at the University of Pennsylvania (a) dull side under 10 000 magnification; (b) dull side under 36 000 magnification; and (c) shiny side under 10 000 magnification

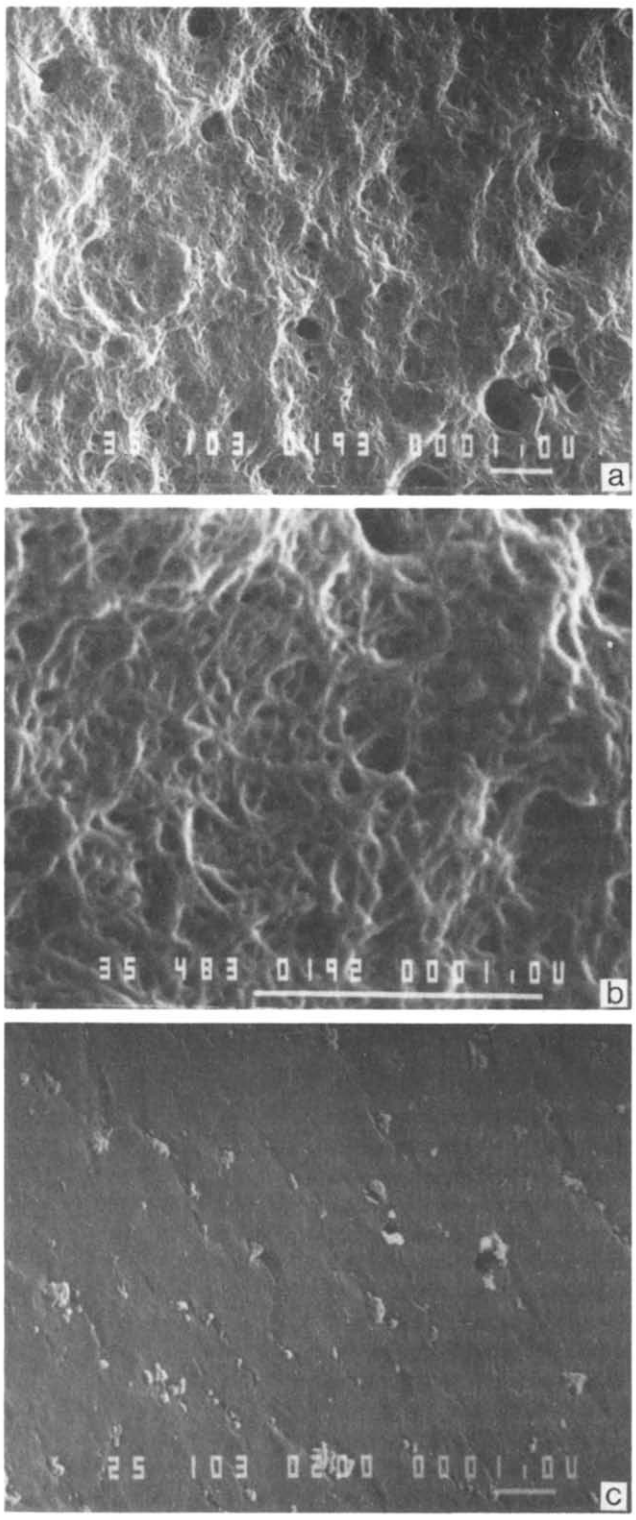

Figure 4 *Trans*-$(CH)_x$ prepared at University of Pennsylvania. (a) Dull side, 10 000 magnification; (b) dull side, 48 000 magnification; (c) shiny side, 10 000 magnification

~400–500 Å. These micrographs demonstrate that the fibril diameter can vary through the film thickness and that samples prepared at different laboratories or from different preparations from the same laboratory can have somewhat different fibril diameters. Pieces of polyacetylene film from this same batch were used for magnetic studies[25,26] of undoped *trans*-$(CH)_x$ and iodine doped $(CH)_x$ (*Figures 5* and *13*).

A third preparation (from the University of Pennsylvania) of *trans*-$(CH)_x$ is shown in *Figure 4*. The low magnification of the dull side reveals fibrils, holes and denser areas, *Figure 4a*. The higher magnification photograph, *Figure 4b*, shows that the fibrils are nearly uniform in their 200 Å diameters. The shiny side is shown at moderate magnification in *Figure 4c*. Here the film is so dense that it appears almost solid. In addition small pieces of non-fibrous material are again observed. Pieces of polyacetylene film from the same batch were used to prepare the arsenic pentafluoride doped films discussed below (*Figures 15*, *16* and *17*).

Effects of doping on morphology (iodine)

Using the $(CH)_x$ films studied in *Figures 2–4*, and similar films, the effects of doping on the morphology were explored. Within the *SEM* imaging resolution (~50 Å) there is no apparent shift away from the fibrous nature of the films upon doping with iodine. However, an increase in fibril diameter is sometimes observed. A *trans*-$(CH)_x$ film taken from the same sheet as the sample shown in *Figure 3* was doped with I_2 to $(CHI_{0.007})_x$ composition. The doping was carried out *in vacuo* by exposure to the vapour pressure of I_2 at room temperature. The film retains its fibrous features. *Figure 5* is an *SEM* photograph of the shiny side of the film taken at high magnification. As is also true in *Figure 3c* for the undoped film, the fibrils appear short and stubby. This is probably due to the projection of the fibrils onto the reactor vessel, so that only short portions of the fibrils are visible. The diameter of these rod-like fibrils is ~350–400 Å, in good agreement with the morphology of the shiny side of the undoped *trans*.

A piece of *trans*-$(CH)_x$ from the same starting film as shown in *Figure 3* was also doped to a composition of $(CHI_{0.16})_x$ using a nitrogen carrier gas to transport the iodine vapour. The dull side of the film is shown in *Figure 6a*, while the shiny side is shown in *Figure 6b*. The dull side is very similar in appearance to the *Figure 3a* of the starting material, except that the fibrils which compose the structure appear swollen beyond the undoped diameter (i.e., swollen to ~300–400 Å diameter from 200 Å diameter). The occasional pieces of non-fibrous material observed in *Figure 3* remain in *Figure 6a*. On the

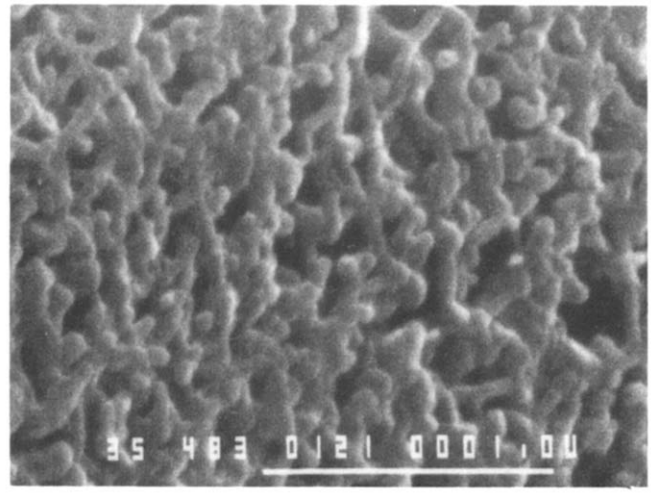

Figure 5 Shiny side of $(CHI_{0.007})_x$ at 48 000 magnification. The undoped *trans* polymer is presented in *Figure 3c*

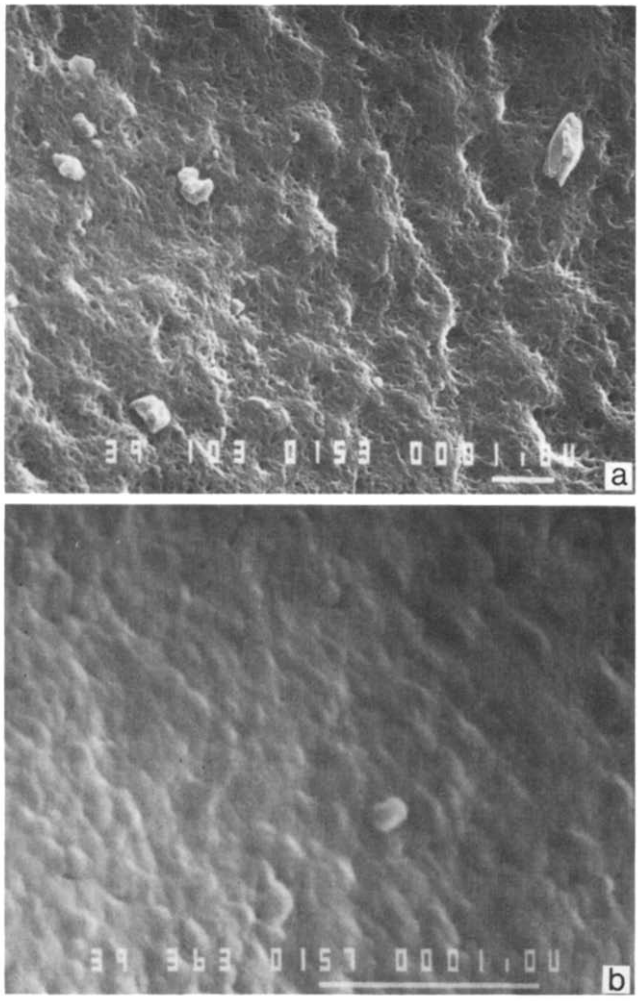

Figure 6 *Trans* polyacetylene doped to $(CHI_{0.16})_x$. (a) Dull side; (b) shiny side

shiny side of the film, the fibrous or rod-like network has swollen to the extent that the film appears continuous with bumps, *Figure 6b*.

Further doping $>16\%$ retains the same features. *Figure 7a* is a high magnification view of the dull side of the heavily iodine doped piece of *trans*-$(CH)_x$ from the same film shown in *Figure 2*. The *trans*-$(CH)_x$ had been stored for $2\frac{1}{2}$ days in an argon atmosphere in the presence of excess iodine. Even at iodine concentration of $>20\%$, the fibrous network is retained. The diameter of the fibrils shown is approximately that of the fibrils displayed in the undoped polymer. This may be due to variation of fibril diameter along the nascent film as well as through the thickness of the film. *Figure 7b* is the shiny side of the same film. Comparison with *Figure 2b* for the shiny side of the undoped polymer demonstrates little change in the morphology except for a swelling of the poorly visible fibrils. The fibrous morphology of heavily iodine doped polyacetylene is confirmed by an *SEM* study of a sample of $(CHI_{0.26})_x$ used for study of matnetic properties[25,26]. *Figures 8a* and *b* illustrate the dull and shiny side morphology of this film. A network of 400–500 Å fibrils is clearly observed on the dull side while the shiny side displays the familiar dense rod-like appearance due to matting of the film against the walls of the polymerization vessel.

Samples of slowly and rapidly iodine doped polyacetylene have been shown to differ in their magnetic properties[25,26]. We examined the morphology of two films of nearly identical iodine concentration $(CHI_{0.133})_x$ and $(CHI_{0.136})_x$. The former film has a very low spin susceptibility ($<2\times10^{-7}$ emu/mole-C) while the latter film has a 'high' spin susceptibility ($\sim2\times10^{-6}$ emu/mole-C). The difference in magnetic behaviour has been attributed to a difference in the radial distribution of dopant through the fibril[25,26]. *Figure 9a* illustrates the shiny side of the $(CHI_{0.136})_x$ sample. It has the typical dense rod-like structure with ~400 Å diameter. The dull side of $(CHI_{0.133})_x$ is displayed in *Figure 9b*. A network of nearly uniform diameter (~300 Å) interconnected fibrils is observed. (Further studies of these films are presented in *Figures 12* and *14* below.) No macroscopic difference in film morphology was observed which could be associated with the difference in magnetic properties. This is consistent with the suggestion[25] of a radial variation in dopant concentration.

Samples used in transport measurements have also been examined. For example, samples of $(CHI_{0.002})_x$, which were shown[27] to have an electric field independent conductivity (for electric field up to 10^4 volts cm^{-1} and temperatures down to 150 K), were inspected under high magnification. The shiny side of this sample again displays the familiar matted rod structure with diameters of ~500 Å (*Figure 10a*). The dull side (*Figure 10b*) had the usual fibril-like network with diameters ~500 Å. In this

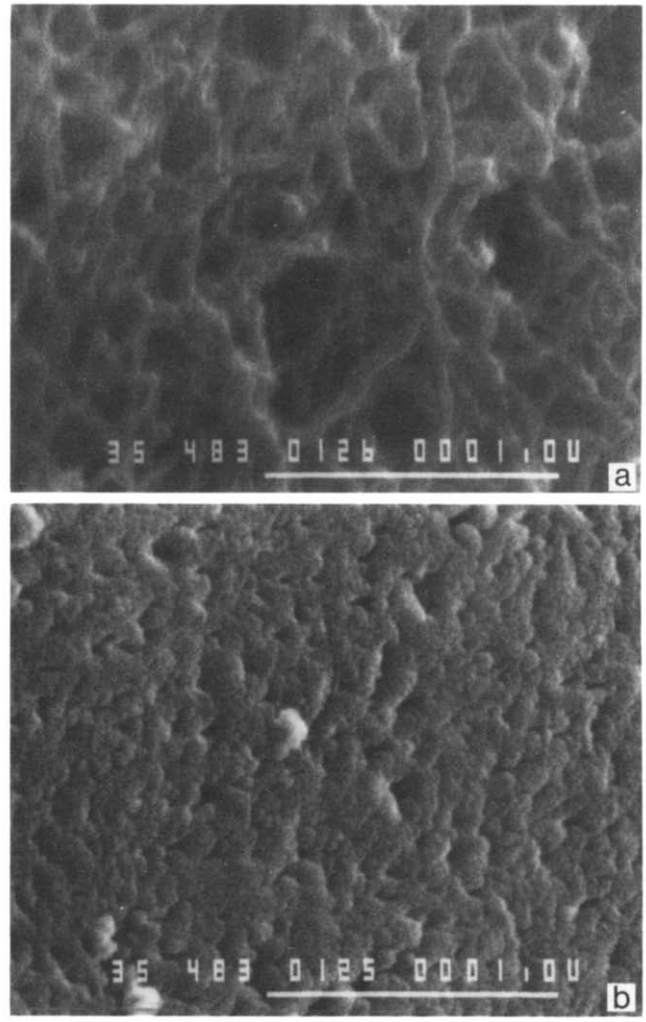

Figure 7 Polyacetylene doped to greater than twenty percent iodine, see text. (a) Dull side; (b) shiny side

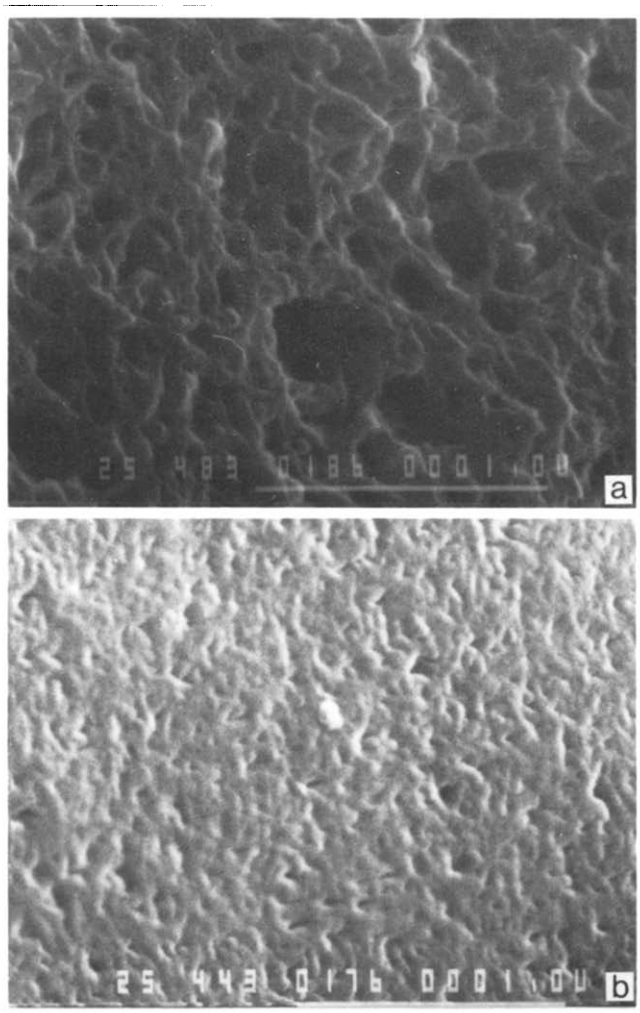

Figure 8 Polyacetylene doped to $(CHI_{0.26})_x$, see text. (a) Dull side; (b) shiny side

photograph, the fibrils appear to be twisted, similar to the twisting of rope. No sign of small metallic particle regions were observed.

Variation of dopant concentration (iodine)

Energy dispersive X-ray analysis (EDXA) was carried out on many of these samples. The resolution of this technique is 5000 Å. This allows us to probe the longer range variation in dopant concentration along the polymer surfaces as well as to determine possible differences in dopant content between the dull and the shiny sides of individual polyacetylene films. Detailed information on dopant segregation within individual fibres is not available through this technique. The results described below demonstrate that any iodine segregation is on a much lower scale than 5000 Å. In the following micrographs the centre solid white line indicates the path scanned by the incident electron beam. The lower line is the approximate zero for the EDXA signal. The rapidly varying line on top is the signal. Only X-rays emitted corresponding to the L lines of iodine were counted. While an absolute concentration is not available, the relative variation of iodine signal along a film as well as comparison of the two sides of the film is meaningful. In a number of cases we have integrated the number of X-ray counts per scan. This integrated number can be compared with scans in other locations on either side of the film to help quantify the variation in iodine distribution. Due to the differing beam settings on different days and the variation in the length of film scanned, the absolute number of counts obtained on the various films cannot be compared to each other.

The EDXA analysis for the $(CHI_{0.002})_x$ film shown in *Figure 10* is given in *Figures 11a* and *b* for the dull and shiny sides respectively. Despite the fibrillar structure a uniform iodine distribution is detected by the EDXA, implying that it is detecting X-rays being emitted by deeper layers in the bulk of the film. The integrated counts for two scans (at different locations) on the dull side yielded very similar values (18 953 counts and 16 269 counts), nearly identical to the values obtained from two scans on the shiny side (18 599 counts and 18 142 counts).

The EDXA of the 'uniformly doped' $(CHI_{0.133})_x$ (shown in *Figure 9b*), demonstrates nearly identical iodine concentrations on the two sides of the film and along the film, *Figure 12*. For two scans on the shiny side, *Figure 12a*, counts of 107 360 and 106 550 were obtained. For the dull side, *Figure 12b*, 102 520 and 101 290 counts were obtained. Hence, the iodine concentrations on the two sides are within five per cent of each other. A study of the $(CHI_{0.26})_x$ sample yielded similar results with 77 676 counts and 81 367 counts on the shiny side compared with 79 154 counts and 77 489 counts on the dull side. No systematic variation was observed as to whether the shiny side had the higher iodine concentration. Generally all

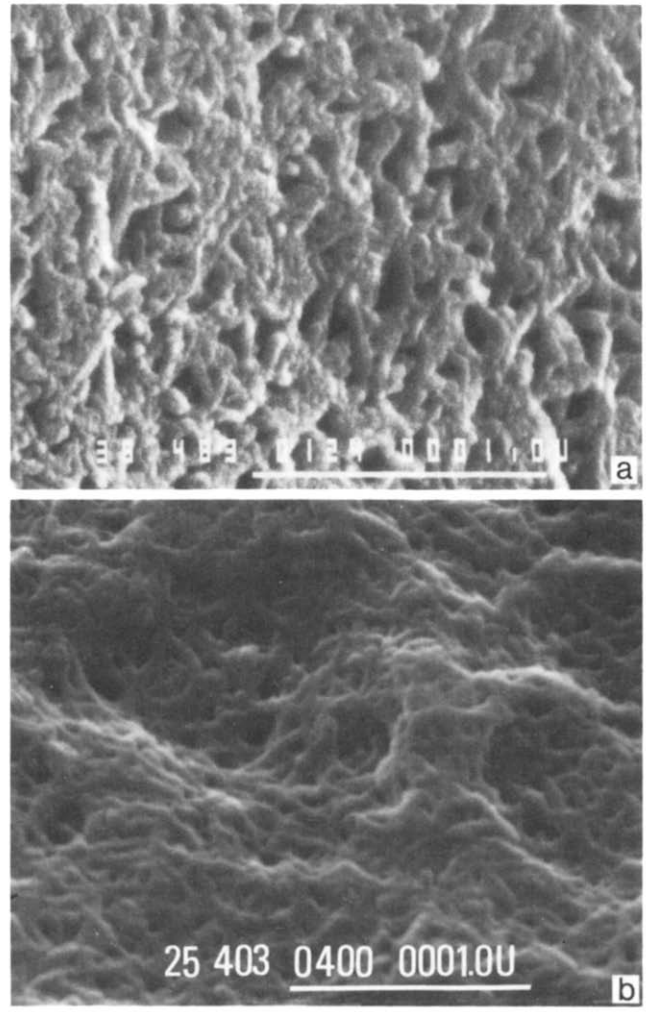

Figure 9 (a) Shiny side of rapidly doped sample of $(CHI_{0.136})$; (b) dull side of slowly doped sample of $(CHI_{0.133})_x$. See text

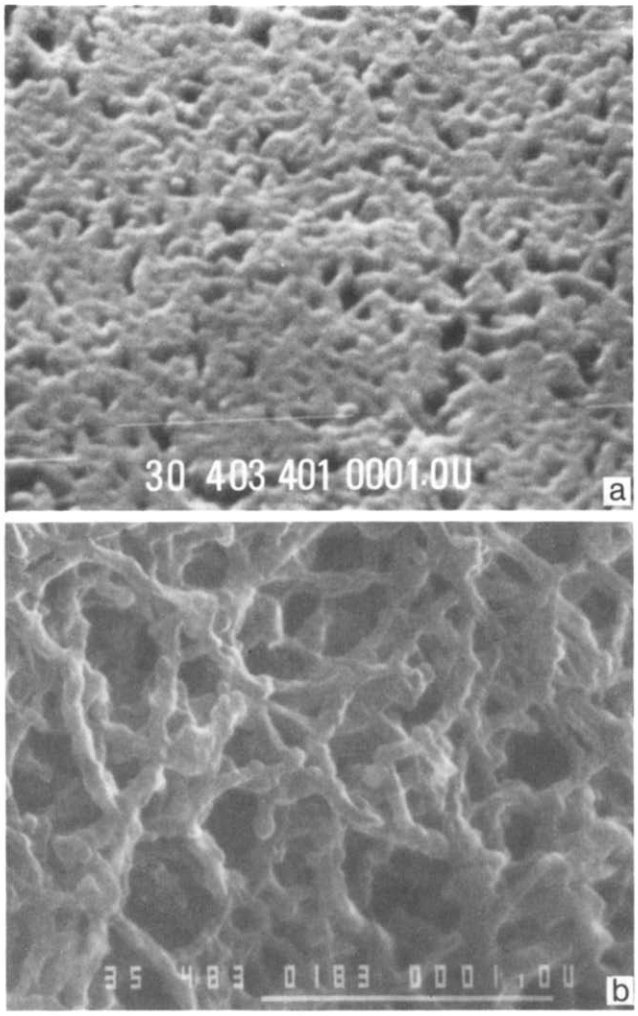

Figure 10 Sample of $(CHI_{0.002})_x$. (a) Shiny side; (b) dull side

areas and both sides of any one film yielded the same results to within 5%.

Samples of $(CHI_{0.16})_x$ (see *Figure 6*) provided an opportunity to test the nature of the non-fibrous material observed on the surface of these films (*Figure 13*). Close examination of *Figure 13a* shows two 'large' (~one micron diameter) pieces of the non-fibrous material in the path of the EDXA scan. The X-ray signal shows no variation upon scanning through these 'lumps'. In fact, EDXA scan counts for two portions of the dull side (63 066 counts and 63 741 counts) compare very well to the total counts taken in two scans of the shiny side (69 770 counts and 71 231 counts). The 10% variation between the two sides is within experimental error of resetting the electron beam currents after removing the sample from the *SEM* in order to invert it. The lack of variation of the EDXA signal upon scanning through the lumps strongly suggests that this is a non-fibrous form of $(CH)_x$ and that it dopes to the same concentration of iodine as the usual $(CH)_x$ fibrils.

In a further effort to detect iodine segregation and/or changes in morphology upon doping, transmission electron microscopic studies of *trans*-$(CH)_x$ and iodine doped $(CH)_x$ were undertaken. This technique requires thin films which are usually obtained by microtome sectioning of samples. In order to section the polyacetylene, samples were potted in epoxy. It was found that the epoxy made it difficult to observe the detailed structure of polyacetylene. In addition, it was observed that iodine diffuses from the doped polyacetylene into the epoxy, further complicating the analysis.

A modified approach can lead to samples suitable for *TEM* study. With care, the epoxy adheres to only one side of the polyacetylene film. Upon microtoming, the side without epoxy is torn revealing areas that are only a single fibril thick. *Figure 14* is a *TEM* photograph (50 000 magnification) of such an area for the $(CHI_{0.136})_x$ film displayed in *Figure 9a*. The *TEM* image density is proportional to the density of the material traversed by the electron beam. The individually observable fibres are of uniform colour. Dark areas appear to be associated with overlapping of fibrils or thicker fibril cross-section. The uniformity in fibril colour indicates that iodine segregation is not present in the individually observable fibrils within the 50 Å *TEM* resolution. The presence of iodine segregation in thicker areas of the film or on a smaller scale cannot be directly determined from these studies.

Morphology and variation of dopant concentration (AsF_5)

The study of morphology and dopant distribution of doped polyacetylene also encompassed $[CH(AsF_5)_y]_x$. All samples for this part of the study were prepared at the University of Pennsylvania. The samples were prepared by doping pieces of *trans*-$(CH)_x$ from the same area of the *trans*-$(CH)_x$ film displayed in *Figure 4*. In addition to the *SEM* images and EDXA, back-scattered electron images

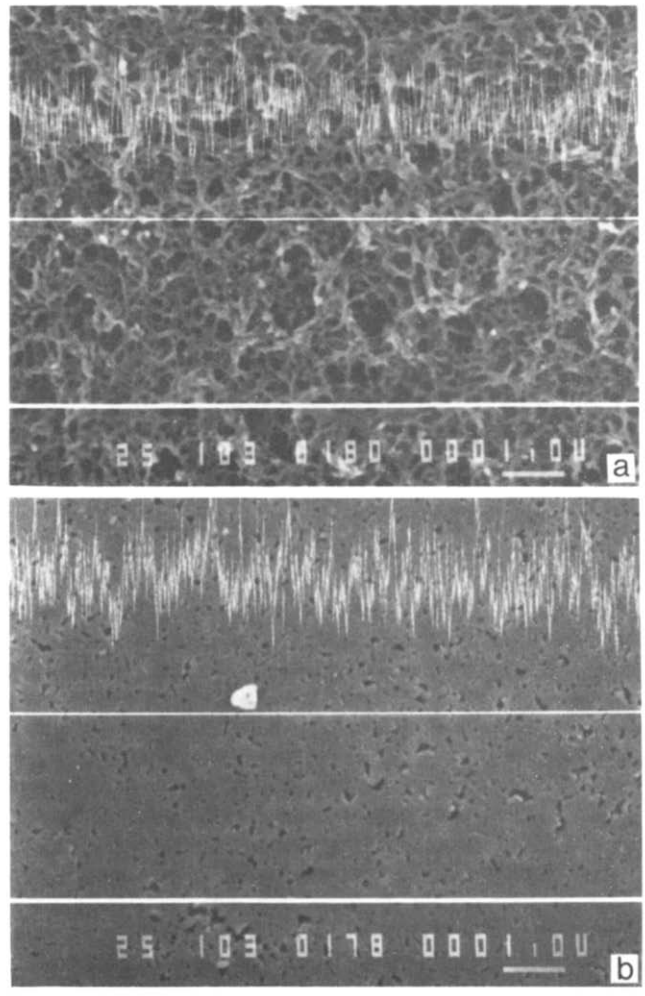

Figure 11 Energy dispersive X-ray analysis (EDXA) of film examined in *Figure 10*. See text. (a) Dull side; (b) shiny side

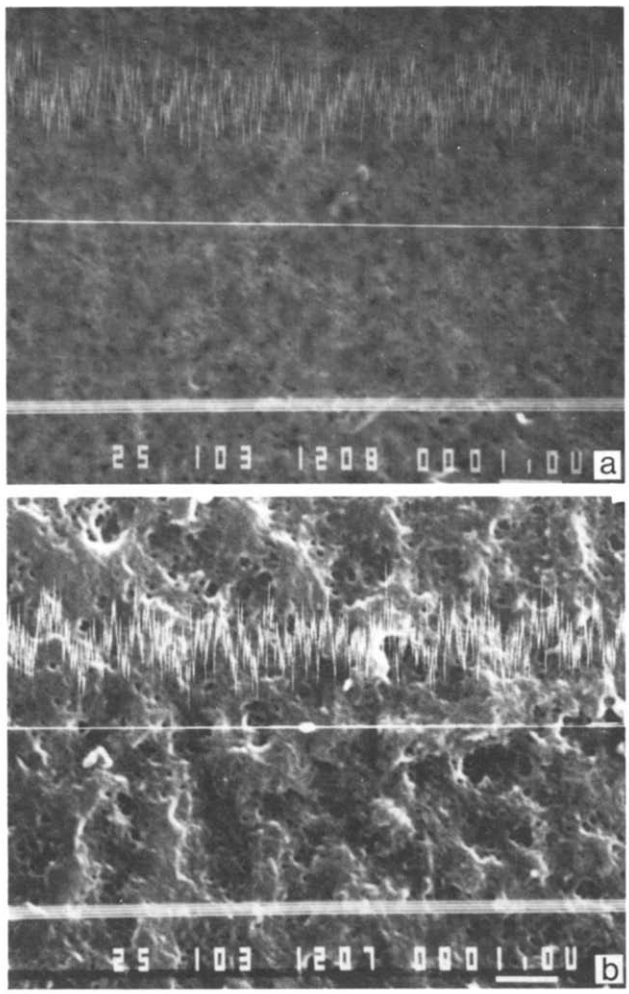

Figure 12 EDXA of 'slowly doped' $(CHI_{0.133})_x$ displayed in *Figure 9b.* (a) Shiny side; (b) dull side

were obtained for these samples in an effort to detect arsenic segregation. As AsF_5 reacts in air, efforts were made to reduce the air exposure of these samples to a minimum (< 5 min). A sample of $(CH(AsF_5)_{0.06})_x$ exposed to air for ~15 min showed signs of oxidation that were not observed for the other samples which were exposed to air for shorter time intervals (see below).

The morphology of rapidly doped $[CH(AsF_5)_{0.01}]_x$ was observed under 20000 magnification. The fibrous network is clearly visible on the dull side, *Figure 15a*, despite the significant amount of matting occurring. Fibril diameter is ~400 Å. The shiny side (*Figure 15b*) displays the typical dense network of ~500 Å diameter rods. These results reveal a significant swelling of the fibril diameter at relatively low AsF_5 concentration, in contrast with the nearly constant fibril diameter observed at the equivalent iodine concentration (*Figures 5* and *10*).

Figures 15c and *d* display the EDXA results for the As distribution for the dull and shiny sides respectively. The As concentration (obtained using the As K_α line) appears uniform across the shiny side of the film (resolution 5000 Å). On the dull side some smooth variation of As concentration is detected, but this may be caused by the very open porous structures of this side.

The *SEM* instrument can also be used to collect the elastically back-scattered electrons. In this mode the image intensity is strongly dependent upon the atomic number of the scattering centres. This technique then gives a means of detecting segregation of the dopant species, although the resolution is limited to ~5000 Å. Back-scattered electron images are shown side by side with the *SEM* image of the dull and shiny side of $[CH(AsF_5)_{0.01}]_x$ in *Figures 15e* and *f*. The results show that the As concentration for any of the features in these photographs is the same as in the average $(CH)_x$. Note the low magnification used, especially in *Figure 15f.*

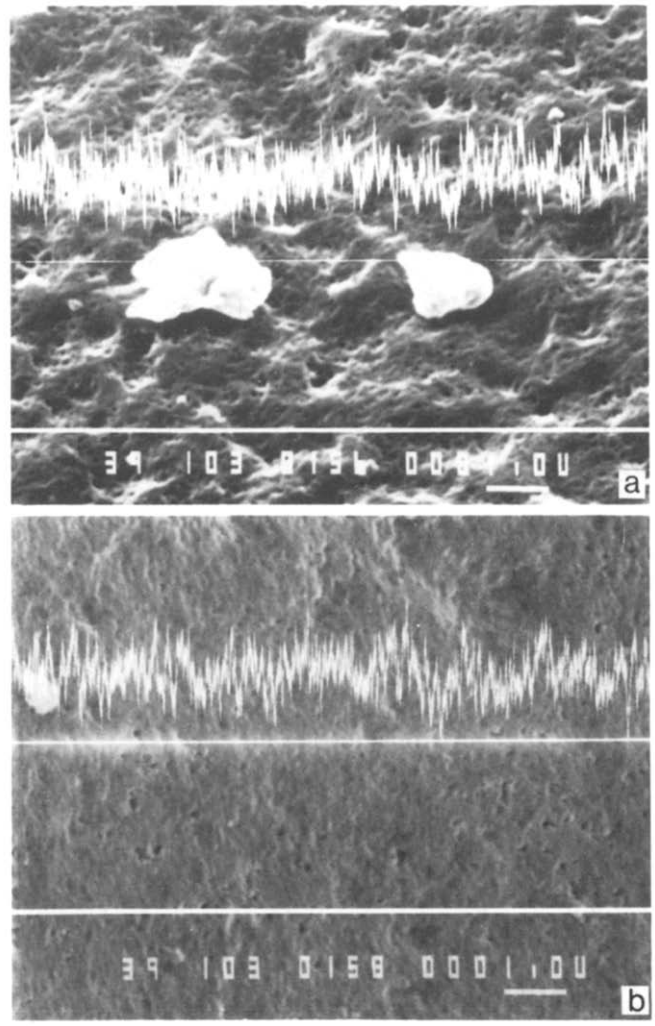

Figure 13 EDXA of $(CHI_{0.16})_x$ examined in *Figure 6*, see text. (a) Dull side; (b) shiny side

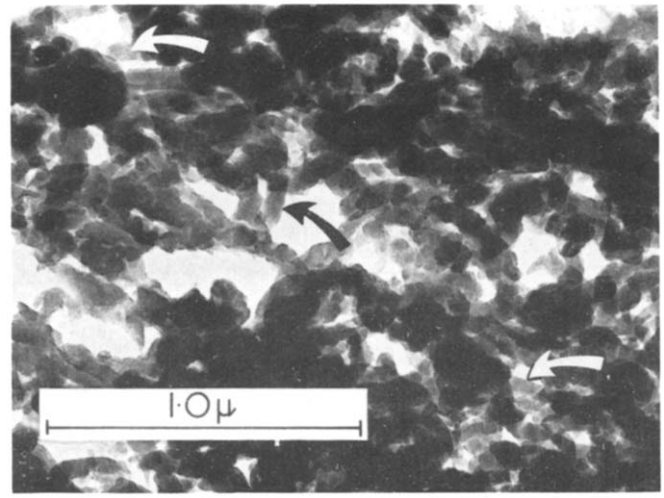

Figure 14 Transmission electron micrograph of $(CHI_{0.136})_x$ examined in *Figure 9a.* The line represents one micron length. The arrows point to single fibril thick regions

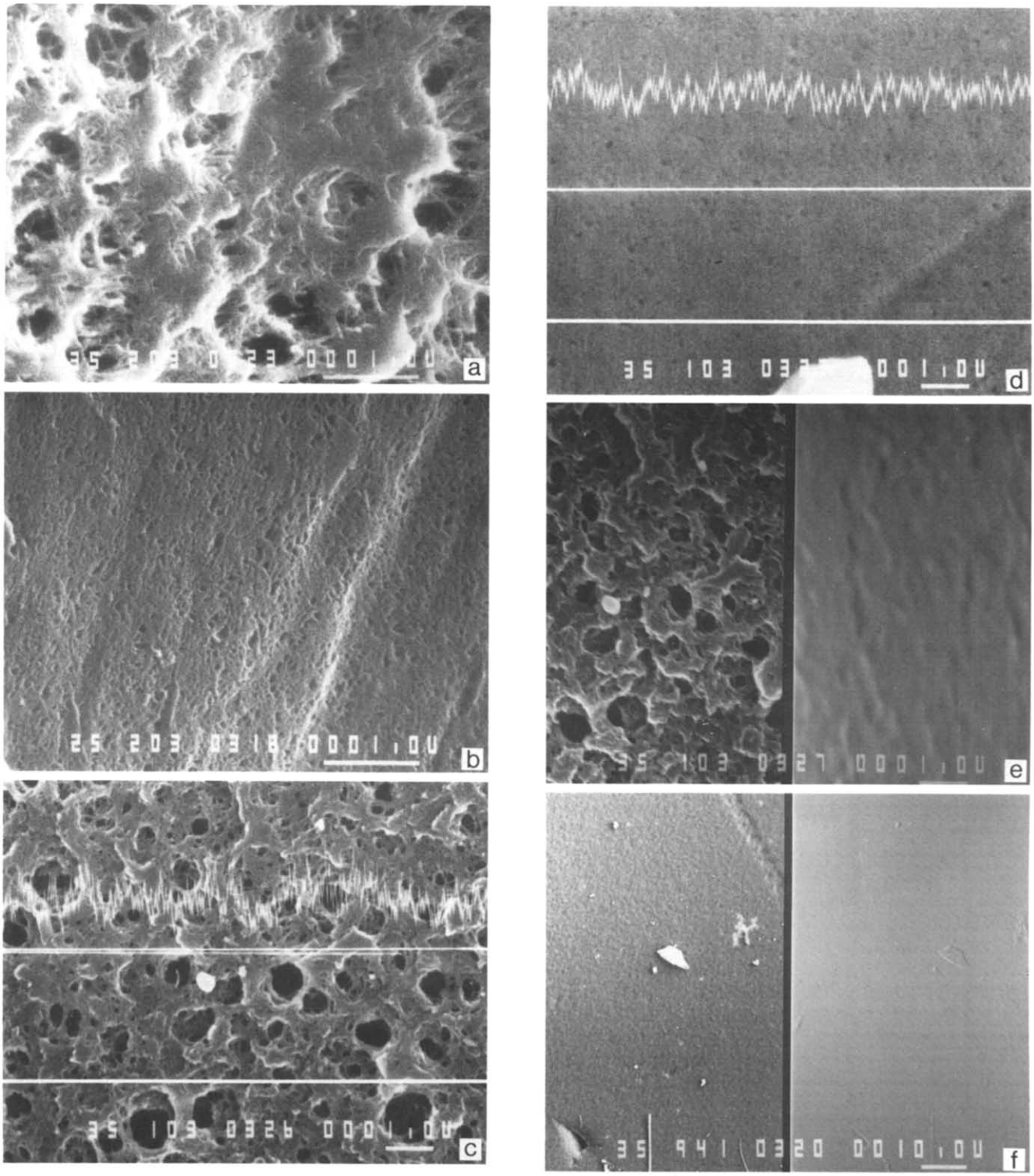

Figure 15 $(CH(AsF_5)_{0.01})_x$ obtained by rapidly doping with AsF_5. (a) Dull side 20 000 magnification; (b) shiny side 20 000 magnification; (c) EDXA of dull side 10 000 magnification; (d) EDXA of shiny side, 10 000 magnification; (e) back-scattered electron image of dull side displayed next to ***SEM*** image of same area (10 000 magnification); (f) back-scattered electron image of shiny side displayed next to ***SEM*** image of same area (941 magnification)

An *SEM* micrograph of the dull side of a rapidly doped sample of $[CH(AsF_5)_{0.039}]_x$ demonstrates that the fibrous structure is retained, however, the fibril diameter increased to ~750 Å, *Figure 16a*. The EDXA for the dull side is typified by *Figure 16b*, which shows that the As distribution is uniform on the 5000 Å scale. The shiny side of this sample, seen in *Figure 16c*, has several striations, probably due to impressions of the striations in the reactor vessel. The EDXA of this side also yields a 'uniform' arsenic distribution, with the same signal intensity as the dull side.

A sample of the *trans*-$(CH)_x$ from the same film examined in *Figures 4*, *15* and *16*, was slowly doped[16] with AsF_5 to a concentration of $[CH(AsF_5)_{0.06}]_x$. The fibrous structure is retained, as seen by examination of the *SEM* micrograph of the dull side, *Figure 17a*. However, a significant further increase in fibril diameter has occurred. The fibrils are smooth and of ~1000 Å diameter. This is

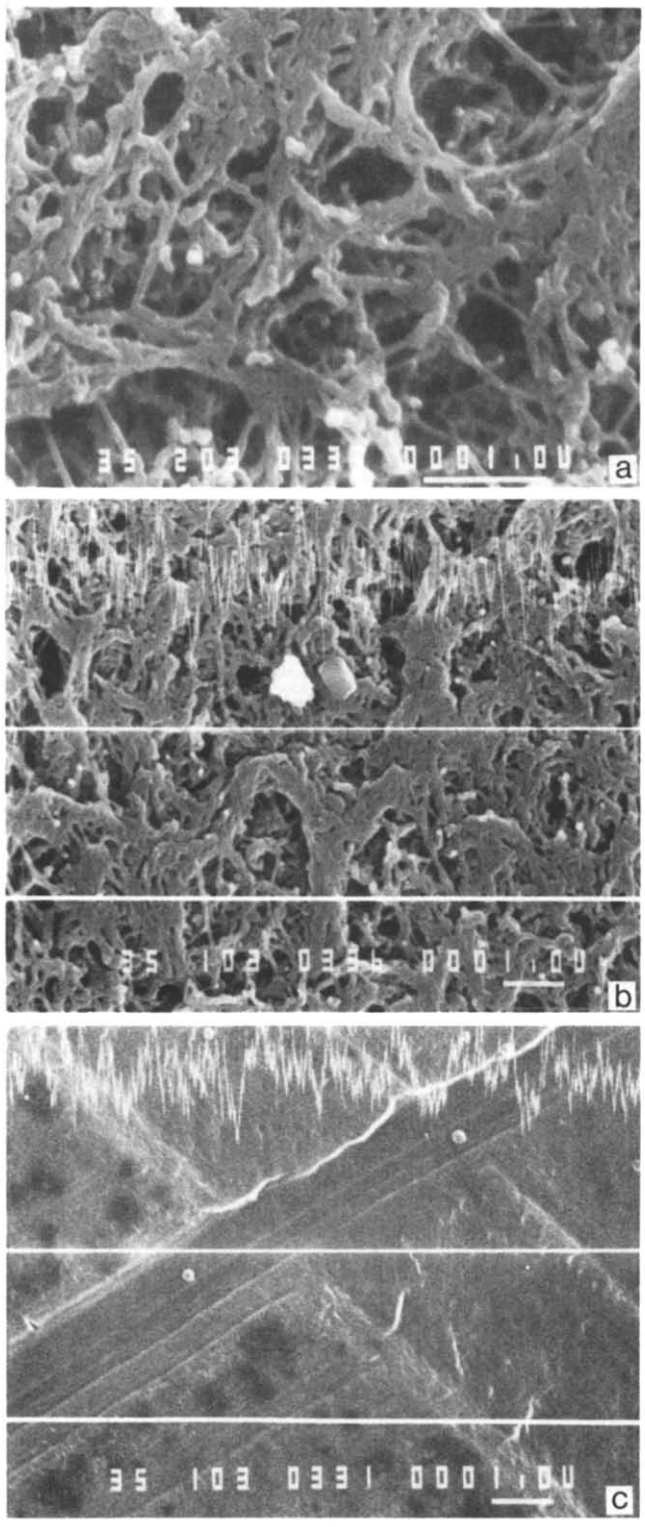

Figure 16 $(CH(AsF_5)_{0.039})_x$ obtained by rapidly doping with AsF_5. (a) Dull side, 20 000 magnification; (b) EDXA of dull side, 10 000 magnification; (c) EDXA of shiny side, 10 000 magnification

considerably greater than the largest expansion observed with iodine doping (*Figure 6*). The very large expansion of the fibril diameter with AsF_5 doping is too large to result only from the intercalation[30] of the dopant molecule into the polyacetylene crystal structure. The intercalation should lead to, at most, a doubling of the fibril diameter. This is in contrast to the iodine results discussed above. The much larger expansion of the fibril diameter of these AsF_5 doped samples may be due to the subsequent conversion of AsF_5 to AsF_6 and the simultaneous evolution of AsF_3 gas[2,31]. A rapid generation of AsF_3 could lead to a puffing up of the polyacetylene fibrils. Further studies are in progress[27] to clarify these differences.

A low magnification view, *Figure 17b*, reveals the presence of rhombohedral shaped crystals imbedded in the fibril network of the $[CH(AsF_5)_{0.06}]_x$ sample. An *SEM* micrograph of the shiny side shows similar 0.5

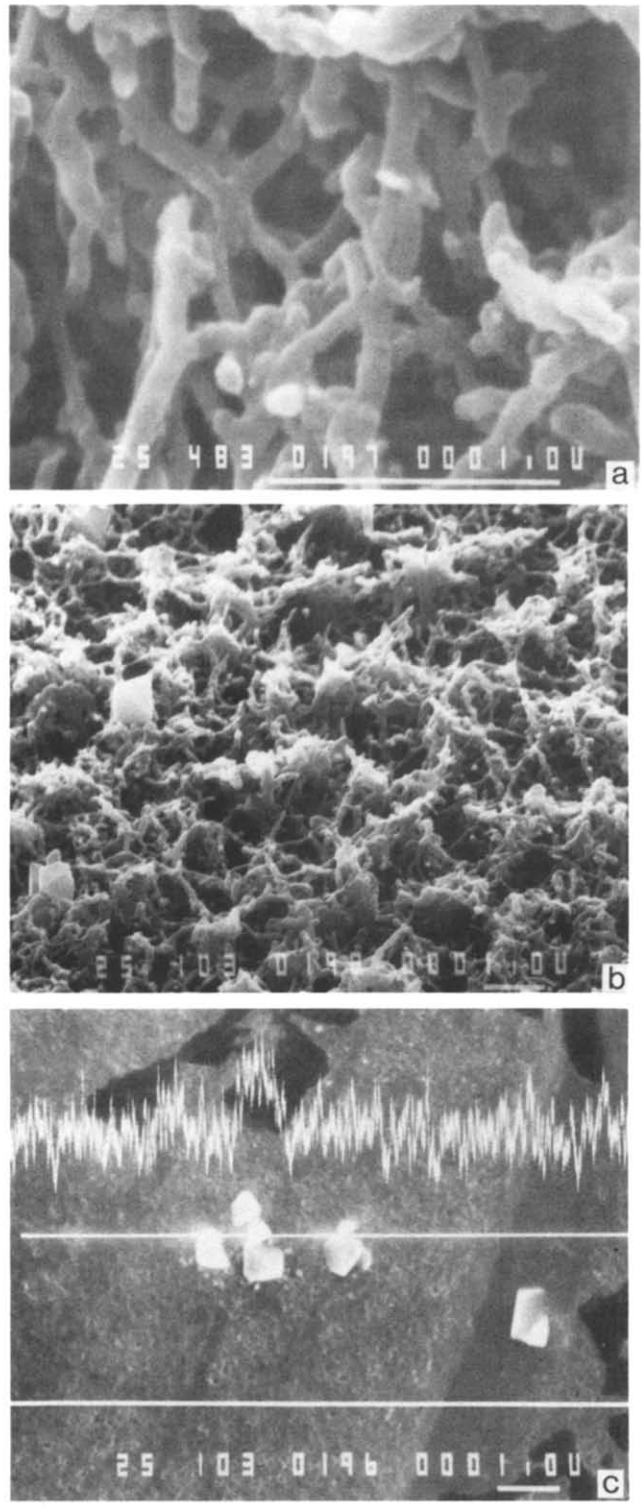

Figure 17 $(CH(AsF_5)_{0.06})_x$ obtained by slowly doping with AsF_5. (a) Dull side, 48 000 magnification; (b) dull side, 10 000 magnification; (c) EDXA of shiny side, 10 000 magnification

micron diameter rhombohedral crystals on the typical dense rod-like structure. The EDXA of the shiny side, reveals a uniform (to 5000 Å resolution) arsenic distribution in the polymer film, and an anomalously large arsenic signal when the scan passes through one of these crystals. Since this sample was exposed to air for more than 15 min during the insertion procedures, it appears that a degradation product has formed, probably As_2O_3. This observation reinforces the importance of avoiding air exposure of AsF_5 doped films.

CONCLUSION

An extensive study of polyacetylene and doped polyacetylene using *SEM*, *TEM*, EDXA and back-scattered electrons has been carried out. The results reveal a variety of fibrillar morphologies. Generally the dull side was observed to be composed of fibrils ranging from 200 to 500 Å diameter for different sample preparations. The shiny sides of the films are matted, giving the appearance of rigid rods of larger diameter than the fibrils of the dull side. In some samples small amounts of nonfibrous material were observed on the surface of the films. The fibril diameter was observed to vary through a film thickness and for samples prepared in different laboratories or in the same laboratory. These different starting morphologies may lead to some variation in the physical and chemical properties of the undoped and doped polymers.

Doping of the polyacetylene appears to cause an increase in the fibril diameter as observed on the rough side. Often, the increase in the diameter on the rod-like smooth side led to filling in of the small amount of open space remaining on the smooth side. This thickening or expansion of the fibrils is qualitatively consistent with the bulk absorption of the iodine and AsF_5 dopants. A quantitative analysis of the increase in the fibril diameter is hampered because of uncertainty in identification of individual fibrils before and after doping. A much more dramatic swelling occurs upon AsF_5 doping than upon iodine doping, possibly related to evolution of AsF_3 gas.

These studies have revealed the growth of small crystals of arsenic rich material upon exposure of AsF_5 doped $(CH)_x$ to the air for a short time (15 min). The growth of these crystals may explain some of the variation in behaviour of $(CH(AsF_5)_y)_x$ reported by workers in the field.

The use of energy dispersive X-ray analysis and back-scattered electron images sets an upper bound for the variation of dopant concentration both along the film and between the two sides of the film. This work demonstrates that any segregation or agglomeration of iodine or AsF_5 is occurring on a scale smaller than 5000 Å diameter. In addition, *TEM* studies of $(CHI_{0.136})_x$ failed to detect iodine segregation even with a 50 Å resolution, in those single fibrils which could be observed.

In conclusion, variations in fibril diameter are observed for different samples of $(CH)_x$. Doping with iodine leads to thickening of the fibrils while doping with AsF_5 leads to a dramatic swelling of the fibrils. Extensive energy dispersive X-ray analysis, back-scattered electron images, and transmission electron microscopic studies have failed to reveal any dopant segregation.

ACKNOWLEDGEMENT

The authors acknowledge extensive discussions with and the cooperation of A. J. Heeger and A. G. MacDiarmid and the cooperation of K. Johnson in providing the *TEM* results. M. A. Druy was supported by National Science Foundation Grant No. DMR 79-23647. T. Woerner was supported by N.S.F. Grant No. DMR 80-22870.

REFERENCES

1 Chiang, C. K., Fincher, C. R., Park, Y. W., Heeger, A. J., Shirakawa, H., Louis, E. J., Gau, S. C. and MacDiarmid, A. G. *Phys. Rev. Lett.* 1977, **39**, 1098
2 For a recent review, see Heeger, A. J. and MacDiarmid, A. G. in 'The Physics and Chemistry of Low Dimensional Conductors', (Ed. L. Alcacer), D. Reidel Publishing Co., Boston, p 353; and MacDiarmid, A. G. and Heeger, A. J. *ibid.* p 393
3 Natta, G., Maxxanti, G. and Corradini, P. *Atti Acad. Nazl. Lincei Rend. Classe Sci. Fis. Mat. Nat.* 1958, **25**, 3
4 Ito, T., Shirakawa, H. and Ikeda, S. *J. Polym. Sci., Polym. Chem. Edn.* 1974, **12**, 11; 1975, **13**,11
5 Karasz, F. E., Chien, J. C., Gralkiewicz, R., Wnek, G. E., Heeger, A. J. and MacDiarmid, A. G. *Nature* 1979, **282**, 286
6 Deits, W., Cukor, P., Rubner, M. and Jopson, H. *J. Electr. Mater.* 1981, **10**, 683
7 Lieser, G., Wegner, G., Müller, W. and Enkelmann, V. *Makromol. Chem., Rapid Commun.* 1980, **1**, 621
8 Luttinger, L. B. *Chem. Ind. (London)* 1960, **36**, 1135; Luttinger, L. B. *J. Org. Chem.* 1962, **27**, 1591
9 Meyer, W. H. *Synth. Met.* in press
10 Lieser, G., Wegner, G., Müller, W., Enkelmann, V. and Meyer, W. H. *Makromol. Chem., Rapid Commun.* 1980, **1**, 627
11 MacInnes, Jr., D., Druy, M. A., Nigrey, P. J., Nairns, D. P., MacDiarmid, A. G. and Heeger, A. J. *J. Chem. Soc. Chem. Comm.* in press
12 Rice, M. J. *Phys. Lett.* 1979, **71A**, 152
13 Su, W. P., Schrieffer, J. R. and Heeger, A. J. *Phys. Rev. Lett.* 1979, **42**, 1698 and *Phys. Rev. B* 1980, **22**, 2099
14 Pople, J. A. and Walmsley, S. H. *Mol. Phys.* 1962, **5**, 15
15 Weinberger, B. R., Kaufer, J., Heeger, A. J., Pron, A. and MacDiarmid, A. G. *Phys. Rev. B* 1979, **20**, 223
16 Ikehata, S., Kaufer, J., Woerner, T., Pron, A., Druy, M. A., Sivak, A., Heeger, A. J. and MacDiarmid, A. G. *Phys. Rev. Lett.* 1980, **45**, 1123
17 Fincher, Jr., C. R., Ozaki, M., Heeger, A. J. and MacDiarmid, A. G. *Phys. Rev. B* 1979, **19**, 4140; Mele, E. J. and Rice, M. J. *Phys. Rev. Lett.* 1980, **45**, 926
18 Suzuki, N., Ozaki, M., Etemad, S., Heeger, A. J. and MacDiarmid, A. G. *Phys. Rev. Lett.* 1980, **45**, 1209
19 Etemad, S., Ozaki, M., Peebles, D. L., Heeger, A. J. and MacDiarmid, A. G. to be published
20 Tomkiewicz, Y., Schultz, T. D., Broom, H. B., Clarke, T. C. and Street, G. B. *Phys. Rev. Lett.* 1979, **43**, 1532
21 Mortensen, K., Thewalt, M. L. W., Tomkiewicz, Y., Clarke, T. C. and Street, G. B. *Phys. Rev. Lett.* 1980, **45**, 490
22 Kuptsis, J. D., Schad, R. G., Tomkiewicz, Y., Clarke, T. C. and Street, G. B. *Bull. Am. Phys. Soc.* 1980, **25**, 161
23 Epstein, A. J., Gibson, H. W., Chaikin, P. M., Clark, W. G. and Gruner, G. *Phys. Rev. Lett.* 1980, **45**, 1730
24 Epstein, A. J., Gibson, H. W., Chaikin, P. M., Clark, W. G. and Gruner, G. *Chemica Scripta* 1981, **17**, 135
25 Epstein, A. J., Rommelmann, H., Druy, M., Heeger, A. J. and MacDiarmid, A. G. *Solid State Commun.* 1981, **38**, 683
26 Epstein, A. J., Rommelmann, H., Druy, M., Heeger, A. J. and MacDiarmid, A. G. to be published
27 Epstein, A. J., Rommelmann, H. and Gibson, H. W. to be published
28 Short, J. M., Fernquist, R. G. and Nixon, W. C. *Scanning Electron Microscopy* 1976, 46 (Chicago, IITRI)
29 Baughman, R. H., Hsu, S. L., Pez, G. P. and Signorelli, A. J. *J. Chem. Phys.* 1978, **68**, 5405
30 Guckelsberger, K., Rodhammer, P., Gmelin, E., Peo, M., Menke, K., Hocker, J., Roth, S. and Dransfeld, K. to be published
31 Clarke, T. C., Geiss, R. H., Gill, W. D., Grant, P. M., Macklin, J. W., Morawitz, H., Rabolt, J. F., Sayers, D. E. and Street, G. B. *Chem. Comm.* 1979, 332